

Experimental demonstration of sidewall angle induced bianisotropy in multiple layer negative index metamaterials

Zahyun Ku^{a)} and S. R. J. Brueck^{b)}

Department of Electrical and Computer Engineering and Center for High Technology Materials, University of New Mexico, Albuquerque, New Mexico 87106, USA

(Received 9 February 2009; accepted 26 March 2009; published online 15 April 2009)

The effect of a nonzero sidewall angle on the performance of multiple layer fishnet-structure (one to three functional layers) negative index metamaterials is evaluated experimentally. The fabrication-induced sidewall angle results in a bianisotropy (inhomogeneous asymmetry) that is significant at optical frequencies. Good agreement is obtained between the experimental transmission and reflectance measurements and the simulation results. Modifications to the standard parameter retrieval algorithm are discussed. © 2009 American Institute of Physics.

[DOI: 10.1063/1.3120223]

The field of metamaterials has seen consistent and rapid growth since the experimental demonstration at radio frequencies.¹ Over the past several years, there has been both experimental and theoretical success in extending magnetic and negative index metamaterials (NIMs) from microwave to optical frequencies.^{2–4} For many applications lower loss is required and research has recently been concentrated on low loss NIMs—(low $Im[n]$) or, equivalently, NIMs with high figures of merit (FOMs) (the FOM is defined the modulus of the ratio of the real and imaginary parts of the effective refractive index). Three-dimensional (multilayered structures approaching bulk properties) rather than two-dimensional (planar) structures are an important emerging research direction toward this goal.^{5–7} However, present fabrication approaches result in significant sidewall angles (SWAs) because the dimensions of optical frequency NIMs require high aspect ratios (vertical/transverse dimensions). In order to fabricate NIMs with one to multiple layers, various lithography approaches, such as interferometric lithography (IL),⁸ e-beam lithography,⁶ focused ion beam (FIB) lithography,⁷ nanoimprint lithography etc., have been used. For the most common processing scheme, the SWA results from the liftoff process used to define the pattern. An array of posts is defined first and the constituent metamaterial films are sequentially deposited followed by a lift-off step to clear the holes in the pattern. The tops of the posts enlarge as the deposition proceeds, with the consequence that the hole diameter also increases with total film thickness. Although FIB is an alternate approach to fabricating NIMs, it also results in a nonzero SWA as discussed in Ref. 7.

In this study, we use gold-based NIMs with elliptical holes, similar to those reported previously in a comparison of unit cell geometry (circle, ellipse, and rectangle).⁹ As a result of the SWA, the NIM structure has a vertical (z -or propagation direction) biasymmetry. The transmission through the structure is identical from either side by reciprocity but the reflectivities are different depending on the incident illumination direction relative to the structural asymmetry. The inhomogeneous asymmetric structure has different S_{11} [reflectivity from port 1 (top, air)] and S_{22} [reflectivity from port 2

(bottom, substrate)] in contrast to the symmetric structure for which $|S_{11}|^2 = |S_{22}|^2$. In order to extract the effective parameters correctly, we have used a modified retrieval algorithm^{10–12} in place of the standard procedure.¹³

The structure of all samples discussed here consists of a BK7 glass ($2.5 \times 2.5 \text{ cm}^2$) substrate with either one (Au/Al₂O₃/Au), two (Au/Al₂O₃/Au/Al₂O₃/Au), or three (Au/Al₂O₃/Au/Al₂O₃/Au/Al₂O₃/Au) functional layers (FLs) perforated with a two-dimensional square array of elliptical holes through the entire structure. Each layer of Au (Al₂O₃) is 25 (58) nm thick, respectively. In brief, the processing steps to fabricate multifunctional layered NIMs with Au/Al₂O₃ are as follows. (A) A thick layer of bottom anti-reflection coating (BARC: XHRIC-16) was spun onto a substrate, followed by a 500 nm thick negative-tone photoresist (NR7–500P). (B) IL using a 355 nm third harmonic YAG:Nd³⁺ laser source was performed to produce periodic elliptical hole arrays (584 and 361 nm in major and minor axes) in the PR layer with two successive one-dimensional (grating) exposures with a 90° rotation of the wafer and different doses for the orthogonal directions. The pitch (830 nm in both directions) is controlled by the angle between the two UV beams and was fixed for all results reported here. (C) A 25 nm thick chromium (Cr) layer was deposited as a selec-

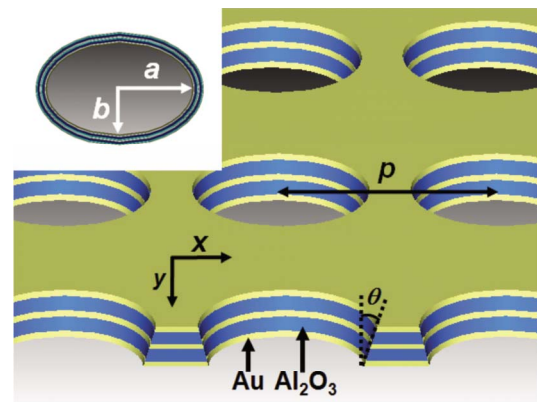


FIG. 1. (Color online) Schematic view of structure and dimensions for two FLs elliptical NIM: $p=830 \text{ nm}$, $2a=584 \text{ nm}$, $2b=361 \text{ nm}$, and $\theta(\text{SWA})=13^\circ$. Inset shows magnified elliptical hole with dimension (a , b) in major/minor axis.

^{a)}Electronic mail: zahyun@chtm.unm.edu. Tel.: 505-272-7800.

^{b)}Electronic mail: brueck@chtm.unm.edu. Tel.: 505-272-7800.

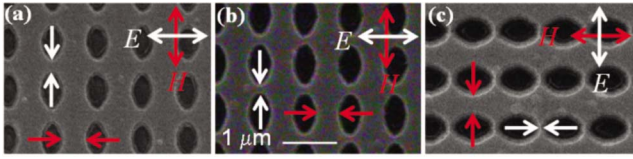


FIG. 2. (Color online) Scanning electron microscope images (top view) of elliptical NIMs with (a) one, (b) two, (c) three FLs. The orientation of polarization is displayed (E and H denote electric and magnetic field, respectively). The increase in the ellipse dimensions with additional layers is clear.

tive etching mask on the developed sample by e-beam evaporation. Lift-off processing resulted in an array of elliptical Cr dots atop the BARC layer, which were used to mask the subsequent etching process. (D) An anisotropic O_2 plasma reactive ion etch with slight isotropic component was used to transfer the Cr pattern into the BARC. The isotropic component results in a slight undercut, which is desirable for the subsequent processing. (E) Next, consecutive e-beam evaporations were used to deposit alternating layers of Au/ Al_2O_3 for one to three FLs. (F) Finally, a high pressure, isotropic O_2 plasma ash was used to remove the BARC posts, leading to final structure, as shown in Figs. 1 and 2. We used an increased thickness of the BARC posts from that in our previous report⁹ to accommodate the increased number of FLs—the total thickness of NIMs with one to three FLs was 108, 191, and 274 nm, respectively.

The transmission and reflectance spectra were recorded with a Nicolet Fourier transform infrared (FTIR) spectrometer with a quartz beam splitter and a DTGS-KBr detector. The transmission measurement was carried out at normal incidence to the samples and was normalized to the transmission through a bare BK7 glass substrate. For reflectance, the input beam is incident on the samples at 11° from the surface normal and normalization is with respect to the reflectivity from a gold mirror. The FTIR beam was polarized along the minor axis of the ellipses as shown in Fig. 2. Measured transmission and reflectance spectra of elliptical NIMs (eNIMs) with one to three FLs are shown in first row of Fig. 3. To simulate the properties of bianisotropy resulting from the fabrication-induced SWA, we used CST Microwave Studio¹⁴ (Computer Simulation Technology GmbH, Darmstadt, Germany) based on a finite integration technique. Appropriate boundary conditions were applied to generate a plane wave propagating along the z -axis as follows. The boundary condition in each unit cell has both a perfect magnetic conductor

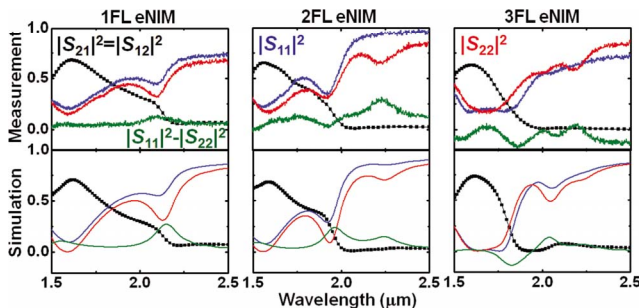


FIG. 3. (Color online) Measured (top) and simulated (bottom) spectra. Transmission— $|S_{21}|^2=|S_{12}|^2$ and reflectance— $|S_{11}|^2$, $|S_{22}|^2$ and $|S_{11}|^2-|S_{22}|^2$ with the specific polarization direction as shown in Fig. 2. The slight blue-shift of the experimental reflectivity resonances is due to the off-normal (11°) measurement angle.

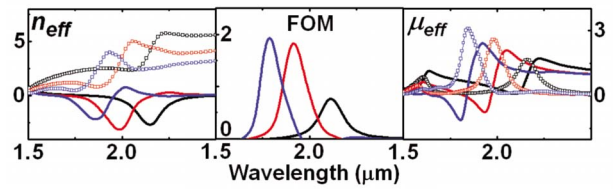


FIG. 4. (Color online) Effective parameters (refractive index, FOM, and permeability) for one to three FLs eNIMs. The color convention is that one FL, two FLs, and three FLs eNIMs are black, red, and blue, respectively. Real (imaginary) part of effective parameters in first and third column is displayed with solid lines (lines with unfilled square).

along the x -axis and a perfect electric conductor along the y -axis. The optical parameters for constitutive materials were taken as $n_{\text{substrate}}=1.5$, $n_{Al_2O_3}=1.62$ and a simple Drude model was used for gold permittivity, with plasma frequency $\omega_p=9.02$ eV, scattering frequency $\omega_c=0.081$ eV, which is three times larger¹⁵ than that reported for bulk gold to give the best fit between experiment and simulation, as shown in Fig. 3. This increased scattering frequency accounts for both additional scattering in the polycrystalline thin films and sample inhomogeneity across the beam diameter.⁹

Previously, a standard method was used to extract isotropic constitutive parameters for a nominally homogeneous symmetric structure. However, the standard retrieval method fails to produce the effective parameters correctly in NIMs with fabrication induced SWAs. In eNIMs with a nonzero SWA, the reflectance depends on the propagation direction of incident beam, $|S_{11}|^2$ (from air) and $|S_{22}|^2$ (from substrate), are different in both experiment and simulation as shown in Fig. 3. The three-dimensional (vector) constituent equation in the (x,y) -plane for eNIMs can be reduced to a 1D equation for the experimental polarization, as illustrated in Fig. 2,¹²

$$D_i = \epsilon_0 \epsilon_i E_i - \frac{i}{c} \xi_0 H_j; \quad B_j = \mu_0 \mu_j H_j + \frac{i}{c} \xi_0 E_i, \quad (1)$$

where $i, j = x, y$ and c , ϵ_0 , μ_0 , and ξ_0 are the speed of light in vacuum, vacuum permittivity, vacuum permeability, and bianisotropic parameter, which are related by $n^2 = \epsilon_i \epsilon_0 \mu_i \mu_0 - \xi_0^2$,¹⁰⁻¹² which results in the correct retrieval of the effective parameters for multiple layered nonvertical sidewall eNIMs. Figure 4 shows the effective refractive index, permeability and FOM for one to three FLs eNIMs using this modified retrieval equation.¹⁰ The eNIM with one FL has a negative $\text{Re}[n_{\text{eff}}]$, negative $\text{Re}[\epsilon_{\text{eff}}]$ (not shown), positive $\text{Re}[\mu_{\text{eff}}]$, and a comparatively large $\text{Im}[\mu_{\text{eff}}]$, which leads to a material with a large loss but nonetheless satisfying the necessary condition for a negative index [$\text{Re}(\epsilon_{\text{eff}})\text{Im}(\mu_{\text{eff}}) + \text{Re}(\mu_{\text{eff}})\text{Im}(\epsilon_{\text{eff}}) < 0$]. The eNIMs with two and three FLs have both $\text{Re}[\epsilon_{\text{eff}}]$ and $\text{Re}[\mu_{\text{eff}}]$ negative, e.g., are double negative materials, and have improved FOMs. An ideal NIM based on the fishnet structure (with vertical sidewalls) has an electric response generated from the array of thin metal wires parallel to the electric field direction (as shown in Fig. 2) and a magnetic response arising from antiparallel induced currents in the array of metal stripes separated by dielectric film (cut wire structure³) along the direction of the magnetic field. In realistic NIMs (with fabrication induced SWAs), the electric dipole is coupled to the magnetic dipole induced by the electric field in the thin metal wires; and in the cut-wire part,

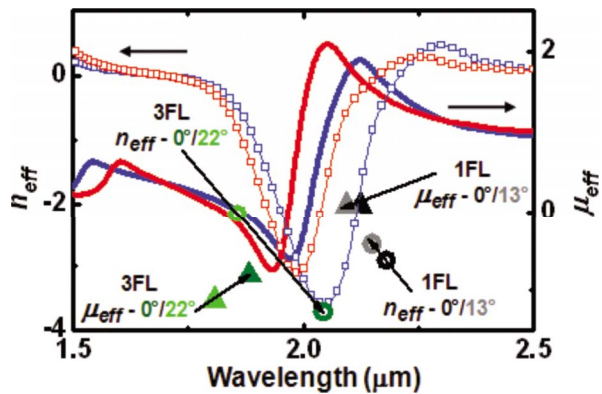


FIG. 5. (Color online) $\text{Re}[n_{\text{eff}}]$ (lines with unfilled squares) and $\text{Re}[\mu_{\text{eff}}]$ (solid lines) in two FLs eNIMs with SWA 0° (blue) and 13° (red). Solid (open) symbols represent $\min(\text{Re}[\mu_{\text{eff}}])$ [$\min(\text{Re}[n_{\text{eff}}])$] of one and three FLs eNIMs with/without SWA. Color convention: gray (black): one FL eNIM with (without) SWA and three FL eNIMs light (dark) green: with (without) SWA.

the magnetic dipole is coupled to a magnetic-field-induced electric dipole. eNIMs with vertical sidewalls were modeled for direct comparison of effective parameters (same as angles used in Figs. 3 and 4).¹² The trend to a decreased wavelength at the $\min(\text{Re}[\mu_{\text{eff}}])$ (cf. Fig. 5) is explained within an equivalent LC circuit model as a reduced capacitance and inductance as the SWA increases, and the decreased magnitude of $\min(\text{Re}[\mu_{\text{eff}}])$ is a result of increased coupling between electric and magnetic dipoles due to the breaking of the symmetric current distribution in the upper and lower metal plates as a result of the reduced width of the upper metal lines. For $\text{Re}[n_{\text{eff}}]$, reduction of the top metal width associated with SWA results in a decrease of absolute value of $\text{Re}[\epsilon_{\text{eff}}]$, which results in a decrease in $\text{Re}[n_{\text{eff}}]$, in addition the change of wavelength at $\min(\text{Re}[n_{\text{eff}}])$ is a result of the blueshifted peaks of $\text{Re}[\mu_{\text{eff}}]$ and $\text{Re}[\epsilon_{\text{eff}}]$.

It is worth pointing out that this understanding of non-zero SWA effects requires correction of our previous report.⁹

As a result of SWA, an $\sim 11\%$ improved FOM is retrieved for the NIMs with rectangular apertures.

In summary, we have investigated effect of nonzero, fabrication induced SWAs on multiple layer elliptical NIMs experimentally and numerically through the effective parameters. The SWA is sensitive to aspect ratio and becomes more significant at optical frequencies. Additional experiments that fully take into account the bi-anisotropy effect due to fabrication imperfection are needed to confirm these sidewall-angle effects with free standing NIMs.

This work was supported by DARPA (contract HR0011-05-1-0006) under the University Photonics Research Center program. We are grateful to Shuang Zhang for technical discussions. Facilities of the NSF (contract 44771-7478) sponsored NNIN node at the University of New Mexico were used for the fabrication.

- ¹R. A. Shelby, D. R. Smith, and S. Schultz, *Science* **292**, 77 (2001).
- ²S. Zhang, W. Fan, N. C. Panoiu, K. J. Malloy, R. M. Osgood, and S. R. J. Brueck, *Phys. Rev. Lett.* **95**, 137404 (2005).
- ³V. M. Shalaev, W. Cai, U. K. Chettiar, H.-K. Yuan, A. K. Sarychev, V. P. Drachev, and A. V. Kildishev, *Opt. Lett.* **30**, 3356 (2005).
- ⁴G. Dolling, C. Enkrich, W. Wegener, C. M. Soukoulis, and S. Linden, *Opt. Lett.* **31**, 1800 (2006).
- ⁵S. Zhang, W. Fan, N. C. Panoiu, K. J. Malloy, R. M. Osgood, and S. R. J. Brueck, *Opt. Express* **14**, 6778 (2006).
- ⁶G. Dolling, M. Wegener, and S. Linden, *Opt. Lett.* **32**, 551 (2007).
- ⁷J. Valentine, S. Zhang, T. Zentgraf, E. Ulin-Avila, D. A. Genov, G. Bartal, and X. Zhang, *Nature (London)* **455**, 376 (2008).
- ⁸S. R. J. Brueck, *Proc. IEEE* **93**, 1704 (2005).
- ⁹Z. Ku and S. R. J. Brueck, *Opt. Express* **15**, 4515 (2007).
- ¹⁰M. S. Rill, C. Plet, M. Thiel, I. Staude, G. von Freymann, S. Linden, and M. Wegener, *Nat. Mater.* **7**, 543 (2008).
- ¹¹X. Chen, B.-I. Wu, J. Au Kong, and T. M. Grzegorzczuk, *Phys. Rev. E* **71**, 046610 (2005).
- ¹²Z. Ku, J. Zhang and S. R. J. Brueck, *Opt. Express* **17**, 6782 (2009).
- ¹³D. R. Smith, S. Schultz, P. Markös, and C. M. Soukoulis, *Phys. Rev. B* **65**, 195104 (2002).
- ¹⁴C. S. T. Studio Suite (www.cst.com).
- ¹⁵M. A. Ordal, L. L. Long, R. J. Bell, S. E. Bell, R. R. Bell, R. W. Alexander, and C. A. Ward, *Appl. Opt.* **22**, 1099 (1983).